JOURNAL OF CATALYSIS 148, 575–586 (1994)

Surface Segregation in Bimetallic Clusters: Statistical–Mechanical Modeling Using Cluster Site Energies

Liqiu Yang and Andrew E. DePristo

Ames Laboratory, U.S.DOE, and Department of Chemistry, Iowa State University, Ames, Iowa 50011

Received Nobember 9, 1993; revised March 29, 1994

A five-state statistical–mechanical model is employed in the present study of surface segregation in 201-atom bimetallic clusters having truncated cubo-octahedral shape. The model uses ideal entropy of mixing and assumes zero heat of mixing. Surface segregation is studied via direct minimization of the free energy without performing Monte Carlo simulations. The effects of size mismatch between atoms of different type are included via a new empirical formula, based upon dimensional scaling arguments, leading to an increase in the surface fraction of larger atoms. We used the corrected effective medium potentials to generate the site energies (interaction energy per atom) used in the model. A complete list of site energies for nine fcc metals is presented for 201-, 586-, 1289-atom clusters and semi-infinite surfaces. In particular, the corner and edge site energies are found to be independent of cluster size. The model reproduced qualitatively the surface and edge–corner segregation results for 11 50%–50% bimetallic clusters generated by atomistic simulations at 600 K that we reported earlier. The remaining difference in results between the model and the simulations is attributed to the effect of nonzero heats of mixing. For systems with very large (>12%) lattice-size mismatch such as Ni–Ag and Cu–Ag, the distortion from the perfect lattice structure is significant according to the simulations; thus, simple modeling involving a few well-defined states is problematic.

INTRODUCTION

Supported bimetallic clusters are used as catalysts for the conversion of automobile exhausts into nontoxic gases and the refinement of crude oil in the petroleum industry (1, 2). These catalysts operate in the form of nanometer scale particles whose activities are influenced drastically by the degree and type of surface segregation (3, 4). Experimental data on such clusters are extremely difficult to obtain, while theoretical predictions of the structure and energies of these clusters depend upon an accurate and computationally efficient description of metal–metal bonding. The study of bimetallic clusters is both important technologically and challenging scientifically.

There have been a number of theoretical calculations (5–8) and simulations (9–14) of small bimetallic clusters reported. These studies range from free-energy minimization (5–7), tight-binding electronic structure theory (8), and rigid-lattice Monte Carlo (MC) simulations (9–11) to continuous molecular dynamics (MD) and Monte Carlo simulations (11–14).

In Ref. (14), we presented the results of atomistic MD and MC simulations on surface segregation in bimetallic clusters of Rh, Ni, Pd, Cu, and Ag. The interaction energies were generated from a simplified version of the non-self-consistent electron-density-functional corrected effective medium (CEM) theory (15), namely, the molecular dynamics/Monte Carlo-corrected effective medium (MD/MC-CEM) theory (15d). Using MC exchange of the positions of unlike atoms in conjunction with continuous MD evolution of all atoms, we reported systematic, quantitative studies of the composition, cluster-size, and temperature dependencies of the surface and edge–corner segregation profiles.

While atomistic simulations provide the most reliable, detailed, and accurate treatments, they suffer from two inherent weaknesses. Computationally, they are very demanding and the demands increase rapidly at low temperatures. Conceptually, it is also difficult to relate simulated results to a few parameters which would enable one to understand the fundamental principals underlying segregation behavior. As such, it is important to seek alternative theoretical tools which, when combined with atomistic simulations, can provide faster results and more insight on surface segregation phenomena.

In this paper, we use a much simpler free-energy minimization approach to study surface segregation in bimetallic clusters. The inputs into this model are the interaction energies of atoms in different binding sites on a cluster and the formula for the ideal mixing entropy. The energy levels are defined from atomistic cluster calculations using either the MD/MC-CEM or the CEM theories. The results of such simple modeling are compared to the direct atomistic simulations reported in Refs. (11, 13, 14).

0021-9517/94 $6.00

THEORY

The thermodynamic free-energy formulas were developed over 2 decades ago for calculating site segregation in binary clusters having multiple binding sites (16). Much later, Strohl and King presented a general thermodynamic model for surface segregation on multicomponent, multilayer crystal surfaces (17). A variation of the multistate model for clusters of finite size is presented here with a detailed consideration of the energies of each state from a microscopic point of view.

We consider a cluster of truncated cubo-octahedral shape since these are stable shapes and since this allows a concrete discussion of the multistate model. Defining a binding site by counting the number of nearest neighbors to an atom in this location, we find there are five different types of binding sites in the cubo-octahedral cluster: (1) 6-coordinated at the corners; (2) 7-coordinated at the edges; (3) 8-coordinated on the (100)-planar face; (4) 9-coordinated on the (111)-planar face; and (5) 12-coordinated in the interior bulk region. Thus, one may model a bimetallic cluster of this shape using a five-state model for each component.

More generally, for a two-component system of A- and B-atoms with "m" different types of binding sites for each component, the constants, variables, and constraints are the following:

Cluster structural quantities	$N_i \equiv$ number of sites of ith type	(m constants)
Compositional quantities	$N_i^A \equiv$ number of A-atoms in the ith site	(m variables)
	$N^A \equiv \Sigma N_i^A \equiv$ total number of A-atoms	(1 constant)
	$N_i^B \equiv$ number of B-atoms in the ith site	(m variables)
	$N^B \equiv \Sigma N_i^B \equiv$ total number of B-atoms	(1 constant)
	$N_i = N_i^A + N_i^B$	(m constraints)
Site energies	$\varepsilon_i^A \equiv$ energy of an A-atom in the ith site	(m constants)
	$\varepsilon_i^B \equiv$ energy of a B-atom in the ith site	(m constants).

Note that the constraint, $N_i = N_i^A + N_i^B$, reflects the fact that each ith site must be occupied by *one and only one* atom.

The free energy is

$$F = E - TS = E - kT \ln \Omega, \qquad [1]$$

where the energy E for an m-state binary system with *zero* heat of mixing is

$$E = \sum_{i=1}^{m} (N_i^A \varepsilon_i^A + N_i^B \varepsilon_i^B). \qquad [2]$$

Using explicit constants and constraints to eliminate the explicit dependence upon $\{N_i^B\}$ and N_m^A, we rewrite Eq. [2] as

$$E = \sum_{i=1}^{m-1} [N_i^A \varepsilon_i^A + (N_i - N_i^A)\varepsilon_i^B] + \left(N^A - \sum_{i=1}^{m-1} N_i^A\right) \varepsilon_m^A + \left[N_m - \left(N^A - \sum_{i=1}^{m-1} N_i^A\right)\right] \varepsilon_m^B. \qquad [3]$$

Upon collecting terms containing N_i^A, this yields

$$E = \sum_{i=1}^{m-1} [(\varepsilon_i^A - \varepsilon_m^A) - (\varepsilon_i^B - \varepsilon_m^B)] N_i^A + \left\{(\varepsilon_m^A - \varepsilon_m^B) N^A + \sum_{i=1}^{m} \varepsilon_i^B N_i\right\}. \qquad [4]$$

The last two terms in Eq. [4], which are in curved brackets, do not depend upon the variation in occupancy of any site and are thus constant for a given cluster size and composition. One has then an energy function of $m - 1$ variables

$$E = E(N_1^A, N_2^A, \ldots, N_{m-1}^A). \qquad [5]$$

For the configurational contribution to the entropy, the phase space counting yields the multiplicity factor as

$$\Omega = \prod_{i=1}^{m} \frac{N_i!}{N_i^A!\,(N_i - N_i^A)!} \qquad [6]$$

$$= \left[\prod_{i=1}^{m-1} \frac{N_i!}{N_i^A!\,(N_i - N_i^A)!}\right] \times \frac{N_m!}{(N^A - \Sigma_{i=1}^{m-1} N_i^A)!(N_m - N^A + \Sigma_{i=1}^{m-1} N_i^A)!} \qquad [7]$$

$$= \Omega(N_1^A, N_2^A, \ldots, N_{m-1}^A). \qquad [8]$$

Therefore,

$$F = E - kT \ln \Omega = F(N_1^A, N_2^A, \ldots, N_{m-1}^A), \qquad [9]$$

and the model has $m - 1$ independent variables $\{N_i^A, i = 1, \ldots, m - 1\}$ for each temperature, cluster size, and composition.

The "effective" energy levels associated with these $m - 1$ independent variables are $\{(\varepsilon_i^A - \varepsilon_m^A) -$

$(\varepsilon_i^B - \varepsilon_m^B)\}$ from Eq. [4]. Letting the mth state correspond to a bulk site, these "effective" energy levels are just the difference in energy between an A-type atom in the ith and bulk sites and a B-type atom in the ith and bulk sites. An equivalent expression, $(\varepsilon_i^A + \varepsilon_m^B) - (\varepsilon_m^A + \varepsilon_i^B)$, can be interpreted as the energy difference between the final and initial configurations of the atoms in the cluster: an A-atom in the bulk site and a B-atom in the ith site as the initial configuration, and an A-atom in the ith site and a B-atom in the bulk site as the final configuration. Thus the "effective" energy represents the energy required to swap an A-atom in the bulk with a B-atom in the ith site. Clearly, if the "effective" energy is positive, it requires more energy to populate the ith site with A-atoms and these sites will be depleted of A-atoms.

The weakness of Eq. [4] involves the lack of any explicit parameters related to the lattice constant of the metal or the size of the atom. Larger atoms segregate to the surface even if the energetics for two metals are the same in order to relieve the large strain energy associated with the compression of larger atoms in the bulk. Alternatively, if one does not compress the bulk, the smaller atoms will not cover the surface entirely and thus second layer atoms will be exposed, thereby leading to an increase in energy. Either way of thinking about the segregation leads to the same conclusion: inclusion of the effect of lattice-size mismatch requires modification of the energy expression in Eq. [4].

The extension we have developed is based purely on dimensional arguments and thus should be considered empirical. We note that for two-dimensional planar surfaces the energy per unit area controls surface segregation in the thermodynamic limit (18). As such, we assume that an inverse scaling with dimension is appropriate, leading to the following empirical modification of Eq. [4]:

$$E_{\text{size}} = \sum_{i=1}^{m-1} \langle a_0 \rangle^{d_i} \left[\frac{\varepsilon_i^A - \varepsilon_m^A}{(a_0^A)^{d_i}} - \frac{\varepsilon_i^B - \varepsilon_m^B}{(a_0^B)^{d_i}} \right] N_i^A. \quad [10]$$

The subscript "size" simply indicates that size dependence is included in this formula. The scaling exponents, $\{d_i\}$, are 0, 1, and 2 for corner, edge, and surface planar sites, respectively. The scaling length is simply the lattice constant, a_0, which provides a measure of the atomic size. The average lattice constant is defined empirically as the fractional arithmetic average:

$$\langle a_0 \rangle = \frac{N^A a_0^A + N^B a_0^B}{N^A + N^B}. \quad [11]$$

Note that the coefficient in front of N_i^A in Eq. [10], the new "effective" energy level for A-atoms in the ith site, now changes with the composition.

This modification distinguishes the site energies in a mixed cluster from those in a pure cluster or surface system. It can only be expected to be accurate when the difference in lattice size is small since the site energies will vary slowly in this case. If the size difference is large, an atom will be in a local environment that is either very compressed or relaxed and thus the distance to its neighbors will be very different from that in the homogeneous system for which the site energies are defined. In this case, the empirical modification in Eq. [10] will not be accurate.

Equation [10] converts to Eq. [4] when $a_0^A = a_0^B$ (i.e., no mismatch), since in this case $\langle a_0 \rangle$ from Eq. [11] equals a_0^A and a_0^B. Note that the choice of $d_i = 2$ in Eq. [10] for a two-dimensional planar surface site is rigorous (18) but this is not generally true for the sites on finite facets of a cluster due to the absence of two-dimensional periodicity. Furthermore, the choice of d_i's for edge and corner sites is a simple guess based upon the local geometry surrounding such atoms. The way to test the appropriateness of this model is by comparison to the results of accurate atomistic simulations.

One can now study surface and site segregation as a function of the temperature, the overall composition, as well as the cluster size by minimizing the free energy in Eq. [9]. As compared to atomistic simulations, the computer time required for free-energy minimization is significantly less and does not increase with decreasing temperature. The latter is a great advantage at low temperature where convergence of atomistic simulations of either Monte Carlo or molecular dynamics type can be very difficult. Moreover, for systems with four states or less ($m \leq 4$), or equivalently, with three independent variable or less, analytical solutions can be obtained for surface and site segregation upon minimization of the free energy.

To perform these free energy minimizations, one requires the "effective" energy levels for either Eq. [4] or Eq. [10], with size effect excluded and included, respectively. These are generated from CEM method (15), a nonself-consistent electron density functional approach presented briefly here. For N atoms $\{A_i, i = 1, \ldots, N\}$, the CEM theory uses the following equations to calculate the interaction energy:

$$\Delta E(\{A_i\}) = \sum_{i=1}^{N} \Delta E_{\text{EXLM}}(A_i; n_i) + \frac{1}{2} \sum_{i=1}^{N} \sum_{j \neq i}^{N} V_c(i,j) + \Delta G(\{A_i\}), \quad [12]$$

$$n_i = \frac{1}{2} \sum_{j \neq i}^{N} \int \frac{n(A_i; \mathbf{r} - \mathbf{R}_i)}{Z_i} n(A_j; \mathbf{r} - \mathbf{R}_j)\, d\mathbf{r}. \quad [13]$$

Here $n(A_i; \mathbf{r} - \mathbf{R}_i)$ is the atomic electron density for atom A_i obtained from Hartree–Fock calculations (19), while

Z_i and $\mathbf{R}_i$ are the atomic number and nuclear position, respectively.

In Eq. [12], the $V_c(i, j)$ term is the Coulomb interaction energy between atoms A_i and A_j and the ΔG term is the kinetic-exchange-correlation correction energy, both dependent only upon the already specified atomic electron densities. The only adjustable part in Eq. [12] is $\Delta E_{\mathrm{EXLM}}(A_i; n_i)$, the embedding energy of atom A_i into a jellium of electron density n_i defined in Eq. [13]. This embedding function was constructed by forcing the CEM result to duplicate (1) the linear muffin tin orbital (LMTO) calcualted bulk cohesive energy curve (15f) and (2) the dimer binding curve in the Morse form generated from the experimental dimer bond length, binding energy, and vibrational frequency (15g). This procedure is developed and implemented in Ref. (15g), to which the interested reader is directed for details.

The calculation of the last term in Eq. [12], ΔG, is thousands of times slower than the calculation of the first two terms. A simplified version of CEM has been developed to overcome this computational expense and to allow applications to large systems (15d). The central approximation is the incorporation of the computationally intensive ΔG term into the ΔE_{EXLM} term in Eq. [12], yielding

$$\Delta E(\{A_i\}) = \sum_{i=1}^{N} \Delta F_{\mathrm{EXLM}}(A_i; n_i) + \frac{1}{2}\sum_{i=1}^{N}\sum_{j\neq i}^{N} V_c(i, j). \quad [14]$$

Here $\Delta F_{\mathrm{EXLM}}(A_i; n_i)$ is the "effective" embedding function which was also fitted to the bulk and dimer properties mentioned earlier (15f–g). Equation [14] defines the MD/MC-CEM potential used in this work, except that for Ir and Rh dimer information was not incorporated due to the lack of data (15g). We should note that the potentials used in Ref. (14) are identical to the ones used in the present work, although we used the notation LMTO in Ref. (14) and did not mention the incorporation of dimer information.

RESULTS AND DISCUSSIONS

We first obtained the site energies $\{\varepsilon_i^A\}$ and $\{\varepsilon_i^B\}$ from atomistic calculations on the pure system. Since the thermodynamic model is based upon the assumption of zero heat of mixing, this is consistent. For each pure metal, 201-, 586-, and 1289-atom cubo-octahedral clusters truncated from the bulk fcc structure were initialized using the bulk nearest neighbor distance at 0 K. For each cluster, a minimization of the MD/MC-CEM interaction energy was performed via the conjugate-gradient method until the maximum force on any atom was less than 10^{-5} eV/bohr. For each 201-atom cluster, this was followed by an additional minimization of the CEM interaction energy until the maximum force on any atom was less than 10^{-2} eV/bohr. The larger upper limit for the force, 10^{-2} eV/bohr, was necessary due to the lowered numerical accuracy of the computationally intensive CEM calculations. Indeed, the minimization of a 201-atom cluster had to be done on a supercomputer when using the CEM generated interaction energy; at a rate of 100 Mflops, the CPU time required for one CEM calculation at each nuclear geometry is $(1 - 100)N^2$ sec, where N is the number of atoms. These energy-minimized clusters maintained the truncated cubo-octahedral geometry. However, each shell of atoms equidistant from the center either contracted or expanded, relative to the initial configuration.

In Table 1, we list the shell-by-shell MD/MC-CEM energies for the 201-atom Pd cluster as an example. Note that the energy of 12-coordinated atoms in different shells can vary by ≈0.2 eV. This is due to both the effect of differing nonnearest-neighbor interactions and the different shell-by-shell contractions or expansions. For use in the free energy minimization model, we define the bulk energy as the arithmetically weighted average energy of all the atoms with coordination 12. These are presented in Tables 2 and 3, e.g., −3.809 eV for Pd (size 201) in Table 2. The variation of even 0.1–0.2 eV in the bulk energy is rather unimportant since it is only the relative difference, $\{(\varepsilon_i^A - \varepsilon_{\mathrm{bulk}}^A) - (\varepsilon_i^B - \varepsilon_{\mathrm{bulk}}^B)\}$, that enters. Similarly, the smaller variations in the (111)-surface and edge site energies in Tables 2 and 3 were also averaged over to provide site energies for atoms with coordinations 9 and 7, respectively.

We should also mention that shells 9*a* and 9*b* have the same distance from the center in a perfect 201-atom cubo-octahedral cluster. They have different energies in Table

TABLE 1

Shell-by-Shell Energies in Units of eV for Pd in a 201-Atom Monatomic Cluster, Calculated Using the MD/MC-CEM Potential

Shell	Number of atoms	Energy	Coordination	Site
0	1	−3.924	12	Bulk
1	12	−3.904	12	Bulk
2	6	−3.871	12	Bulk
3	24	−3.842	12	Bulk
4	12	−3.810	12	Bulk
5	24	−3.709	12	Bulk
6	8	−3.155	9	(111)
7	48	−3.125	9	(111)
8	6	−3.052	8	(100)
9*a*	24	−2.740	7	Edge
9*b*	12	−2.662	7	Edge
10	24	−2.445	6	Corner

TABLE 2

MD/MC-CEM Site Energies in Units of eV for Relaxed Clusters and Surfaces
(C = Coordination Number)

Metal	Size	C = 12 bulk	C = 9 (111)	C = 8 (100)	C = 7 edge	C = 6 corner
Al	201	−3.319	−2.964	−2.928	−2.719	−2.530
	586	51	81	926	5	1
	1289	63	87	924	2	0
	∞	89	88	894	—	—
Ni	201	−4.348	−3.608	−3.522	−3.158	−2.875
	586	386	25	31	62	4
	1289	402	31	33	62	2
	∞	440	41	19	—	—
Cu	201	−3.425	−2.879	−2.814	−2.531	−2.303
	586	53	892	815	1	2
	1289	64	896	815	0	1
	∞	90	902	795	—	—
Rh	201	−5.621	−4.705	−4.611	−4.151	−3.788
	586	675	30	28	7	6
	1289	698	39	33	7	3
	∞	750	57	19	—	—
Pd	201	−3.809	−3.129	−3.052	−2.714	−2.445
	586	43	45	61	7	3
	1289	57	50	64	7	1
	∞	90	61	55	—	—
Ag	201	−2.911	−2.487	−2.431	−2.220	−2.041
	586	28	496	6		39
	1289	34	500	7		37
	∞	50	505	1	—	—
Ir	201	−6.785	−5.762	−5.667	−5.126	−4.702
	586	850	791	74	30	2
	1289	877	801	74	29	1
	∞	939	812	34	—	—
Pt	201	−5.750	−4.942	−4.859	−4.477	−4.184
	586	787	60	67	82	2
	1289	802	66	70	83	0
	∞	838	78	62	—	—
Au	201	−3.755	−3.163	−3.092	−2.810	−2.587
	586	780	75	90		6
	1289	790	79	90		5
	∞	811	87	78	—	—

1 because edge atoms in shell 9*a* bridge the (100) and (111) facets, while edge atoms in shell 9*b* bridge two adjacent (111) facets. The (100)-surface site energy in Table 1 has only a single value, which is the case only for 201- and 586-atom clusters. In a 1289-atom cluster, there are three different types of (100)-surface sites which have slightly different energies. The only type of site that does not require any averaging for the site energy for all cluster sizes is the corner site. There are always 24 identical corner sites in a truncated cubo-octahedral cluster of any size. The numbers of other types of sites in 586- and 1289-atom clusters are: 72 and 108 for edge, 24 and 54 for (100), 152 and 296 for (111), and 314 and 807 for bulk.

In Tables 2 and 3, we provide a complete list of the MD/MC-CEM and CEM site energies for Al, Ni, Cu, Rh, Pd, Ag, Ir, Pt, and Au, generated using the above procedure for 201-, 586-, and 1289-atom clusters. These two tables provide a vast increase in the amount of information available about bonding in these systems. For the site energies of 586- and 1289-atom clusters and infinite (∞) systems, only the digits *different* from the 201-atom values of the same metal and same site are shown while the initial digits identical to the 201-atom values are left blank for clarity.

First, we should point out an unusual behavior in Table 2; the low coordination site energies for Al are more negative than those for Cu, even though Al is bound weaker than Cu in the bulk. This is an artifact of the flatness of $\Delta F_{\mathrm{EXLM}}(\mathrm{Al}; n)$ in the jellium density region between the dimer and the bulk. The first derivative of the MD/MC-CEM embedding function for Al exhibits a minimum in this intermediate electron density region, thus overly sta-

TABLE 3

CEM Site Energies in Units of eV for Relaxed Clusters and Surfaces (C = Coordination Number)

Metal	Size	C = 12 bulk	C = 9 (111)	C = 8 (100)	C = 7 edge	C = 6 corner
Al	201	−3.324	−2.866	−2.834	−2.555	−2.336
	∞	88	89	06	—	—
Ni	201	−4.307	−3.771	−3.747	−3.404	−3.132
	∞	439	819	3	—	—
Cu	201	−3.396	−2.978	−2.967	−2.693	−2.475
	∞	489	−3.004	43	—	—
Rh	201	−5.593	−4.851	−4.811	−4.368	−4.017
	∞	746	910	4	—	—
Pd	201	−3.788	−3.238	−3.201	−2.877	−2.610
	∞	887	75	12	—	—
Ag	201	−2.891	−2.542	−2.534	−2.314	−2.129
	∞	946	67	37	—	—
Ir	201	−6.769	−5.874	−5.797	−5.260	−4.831
	∞	935	919	51	—	—
Pt	201	−5.744	−5.048	−4.986	−4.613	−4.321
	∞	834	75		—	—
Au	201	−3.744	−3.274	−3.235	−2.965	−2.750
	∞	804	92	22	—	—

bilizing the low coordination sites in a cluster. This is due to the fact that the embedding function based on dimer data and the one based on LMTO bulk calculations differ significantly, making it difficult to join them smoothly.

The values of bulk site energies for infinite (∞) size clusters are taken as the bulk cohesive energies of metals which are reproduced exactly by both MD/MC-CEM and CEM models (15f–g), while those for the (111) and (100) site energies were taken as the potential energy of the corresponding first-layer atom obtained by atomistic calculations of relaxed two-dimensional surfaces. In such calculations, the top seven layers were allowed to adjust their vertical positions, while the bottom three layers for (111) and the bottom four layers for (100) were held rigid at the bulk separations. We did not include energies of subsurface (second- and third-layer, etc.) atoms to obtain an averaged value for the bulk energy in the surface calculations for two reasons. First, subsurface atoms on (111) and (100) surfaces have different energies, precluding a unique choice. Second, a real surface has infinitely many layers which would produce an average bulk site energy equal to the bulk cohesive energy unless some arbitrary cutoff was invoked. Since the bulk site energy is not critical, we decided to consistently include only atoms with coordination 8 for (100) and 9 for (111), i.e., the top layer atoms. The ambiguity in coordination for open surfaces makes the edge and corner site energies for an infinite (∞) size system ill-defined and thus these were not calculated.

Perhaps the most striking feature of Table 2 is the very small variation in corner energy with cluster size: for an increase from 201 to 1289 atoms, the largest change is only 5 meV for Rh. Correspondingly, the largest change in the edge energy is only 7 meV for Al. This absence of cluster-size dependence for the corner and edge site energies in nanometer clusters implies that the local bonding arrangement is the dominant factor determining these interactions. By contrast, the bulk and (111) site energies decrease with increasing system size due to the increasing number of non-nearest neighbors which contribute to the attractive interactions. The (100) site energy, however, increases by 34 meV for Al and 33 meV for Ir as the size increases from 201 to ∞ in Table 2. We have not discovered any satisfactory explanation for this behavior, which deviates from that of most other metals.

Although Table 2 contains only MD/MC-CEM results, it is quite plausible that the lack of cluster-size dependence for corner and edge site energies is universal. As such, we expect that the CEM corner and edge site energies generated from 201-atom clusters in Table 3 could also be used for much larger clusters, say 1289 atoms, for which direct energy minimizations are too demanding computationally.

On the other hand, to judge from Table 2, using the bulk and surface site energies of 201-atom clusters directly for 1289-atom clusters would not be so reliable. The infinite-size limiting values for the CEM bulk cohesive energy and surface site energies are already available in Table 3. The variation for each system is very similar in the MD/MC-CEM and CEM results from size 201 to ∞. For simplicity, one may assume that between CEM and MD/MC-CEM, the variation in site energies from one cluster size to another only differs by a constant which can be determined by the 201 and ∞ values in Tables 2 and 3.

Such a simple interpolation procedure will provide CEM bulk and surface site energies for each cluster size.

With the site energies available, we now compare results of the direct free-energy minimization model with those from atomistic simulations. We first show the surface and edge-corner segregation results for ten 50%–50% bimetallic clusters in Table 4 which is in the same format as Table 2 of Ref. (14). In accord with the convention used in Ref. (14), the surface percentages include contributions from all non-bulk sites. The results from the model without size effect and the model with size effect were generated using Eq. [4] and Eq. [10], respectively, for the total energy of a bimetallic cluster. For the latter, the lattice constants in Å that were used for the metals are 4.09 (Ag), 4.08 (Au), 4.05 (Al), 3.92 (Pt), 3.89 (Pd), 3.84 (Ir), 3.80 (Rh), 3.61 (Cu), and 3.52 (Ni). The size mismatch is also given in Table 4 for the convenience of the reader. In the analysis of this table, we shall disregard any differences less than 2% for surface and 4% for edge–corner percentages since the atomistic simulations are unlikely to be more accurate than this.

The results in Table 4 fall naturally into four classes based upon the size mismatch and the spacing of the "effective" energy levels, or the difference in surface energies. The first class, consisting of the Rh–Ag, Rh–Cu, and Pd–Ag systems, exhibits medium mismatch of 5–10% and large spacing of 'effective' energies. Shown in Fig. 1 are the "effective" energy levels for Rh–Ag, combined from the MD/MC-CEM site energies for size 201 in Table 2. The spacing of over 0.5 eV between bulk and surface planes is very large compared to the temperature of 600

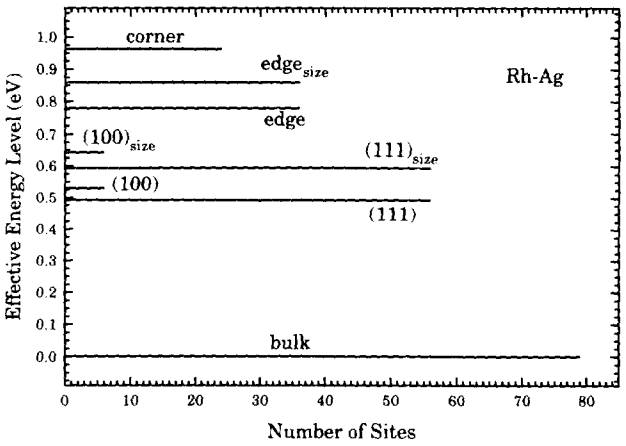

FIG. 1. MD/MC-CEM effective energy diagrams for 201-atom Rh–Ag clusters. The energy levels without subscript "size" were calculated using Eq. [4] with A = Rh and B = Ag for any composition, while the (111), (100), and edge levels with subscript "size" were calculated using Eq. [10] with $N^{Rh} = N^{Ag}$ in Eq. [11], i.e., for a 50%–50% composition. The bulk and corner energy levels are the same in both models.

TABLE 4

The Percentage of Surface (Upper Right) and Edge–Corner (Lower Left) Sites Occupied by the Element with Higher Surface Energy in 201-Atom Bimetallic Clusters at 600 K with 50%–50% Total Concentration

	Rh	Ni	Pd	Cu	Ag	Method
Rh	—	21	18	17	17	Model w/o size, Eq. [4]
	—	32	17	17	17	Model with size, Eq. [10]
	–	40	18	18	18	Atomistic, Ref. (14)
	(0.0)	(7.7)	(2.3)	(5.1)	(7.4)	(Size mismatch)
Ni	3	—	35	20	17	Model w/o size, Eq. [4]
	5	—	23	18	17	Model with size Eq. [10]
	15	—	31	19	5	Atomistic, Ref. (14)
	(7.7)	(0.0)	(10.0)	(2.5)	(15.0)	(Size mismatch)
Pd	2	27	—	24	18	Model w/o size, Eq. [4]
	2	32	—	34	17	Model with size, Eq. [10]
	0	27	—	39	18	Atomistic, Ref. (14)
	(2.3)	(10.0)	(0.0)	(7.5)	(5.0)	(Size mismatch)
Cu	0	3	10	—	25	Model w/o size, Eq. [4]
	0	5	12	—	19	Model with size, Eq. [10]
	0	3	22	—	13	Atomistic, Ref. (14)
	(5.1)	(2.5)	(7.5)	(0.0)	(12.5)	(Size mismatch)
Ag	0	0	2	8	—	Model w/o size, Eq. [4]
	0	3	2	13	—	Model with size, Eq. [10]
	0	0	0	2	—	Atomistic, Ref. (14)
	(7.4)	(15.0)	(5.0)	(12.5)	(0.0)	(Size mismatch)

Note. The metals listed in descending order of surface energy are Rh, Ni, Pd, Cu, Ag. The first, second, and third rows for each bimetallic combination are results from the model without size effect in Eq. [4], model with size effect included in Eq. [10], and atomistic simulations (14) using the MD/MC-CEM interactions, respectively. The last row is the percentage lattice mismatch defined as $200 \times |a_0 \text{ (large)} - a_0 \text{ (small)}|/\{a_0 \text{ (large)} + a_0 \text{ (small)}\}$.

K ($kT \approx 0.05$ eV). The two models agree with the atomistic simulation for trivial reasons: the cluster retains the cubo-octahedral shape (e.g., Rh–Ag in Fig. 2a) and the surface segregation is limited for a 50%–50% mixture in this geometry to 17% (14).

The second class, consisting of the Ni–Ag and Cu–Ag systems, is much more interesting with large mismatch of >10% and variable spacing of "effective" energies (large for Ni–Ag and small for Cu–Ag). The models agree with each other for Ni–Ag but severely underestimate the surface fraction of Ag. The picture in Fig. 2b shows that the atomistic simulation leads to a severe distortion of the Ni–Ag cluster geometry, allowing for a much larger fraction of Ag. Hence, using the simple multiple-state models to describe this system is inaccurate, since there are no well-defined lattice sites in the system. Atomistic simulations are necessary for such systems with large lattice-size mismatch. It is not surprising that the models do not reproduce the simulated results for surface and edge-corner segregation for Ni–Ag and Cu–Ag in Table 4.

The third class, consisting of the Rh–Pd and Ni–Cu systems, exhibits small mismatch of <5% and medium spacing of "effective" energies. The "effective" energy levels for Rh–Pd and Ni–Cu are very similar to Fig. 1 for Rh–Ag, but scaled by approximately a factor of 0.5 for the former and 0.4 for the latter. The models agree with each other because of the small mismatch and also agree with the atomistic simulations. The picture of Ni–Cu in Fig. 2c shows that the cubo-octahedral shape is retained.

The fourth class, consisting of the Rh–Ni, Ni–Pd, and Pd–Cu systems, exhibits medium mismatch of 5–10% and medium spacing of "effective" energies as shown in Fig. 3. The picture of Ni–Pd in Fig. 2d shows that the cubo-octahedral shape is still retained even with a mismatch of 10%. The models disagree with each other because of the medium mismatch. The model without size effect predicts the degree of surface segregation in Ni–Pd (35%) to be much *less* than that in Rh–Ni (21%) and that in Pd–Cu (24%). By contrast, the model with size effect predicts the surface segregation in Ni–Pd (23%) to be

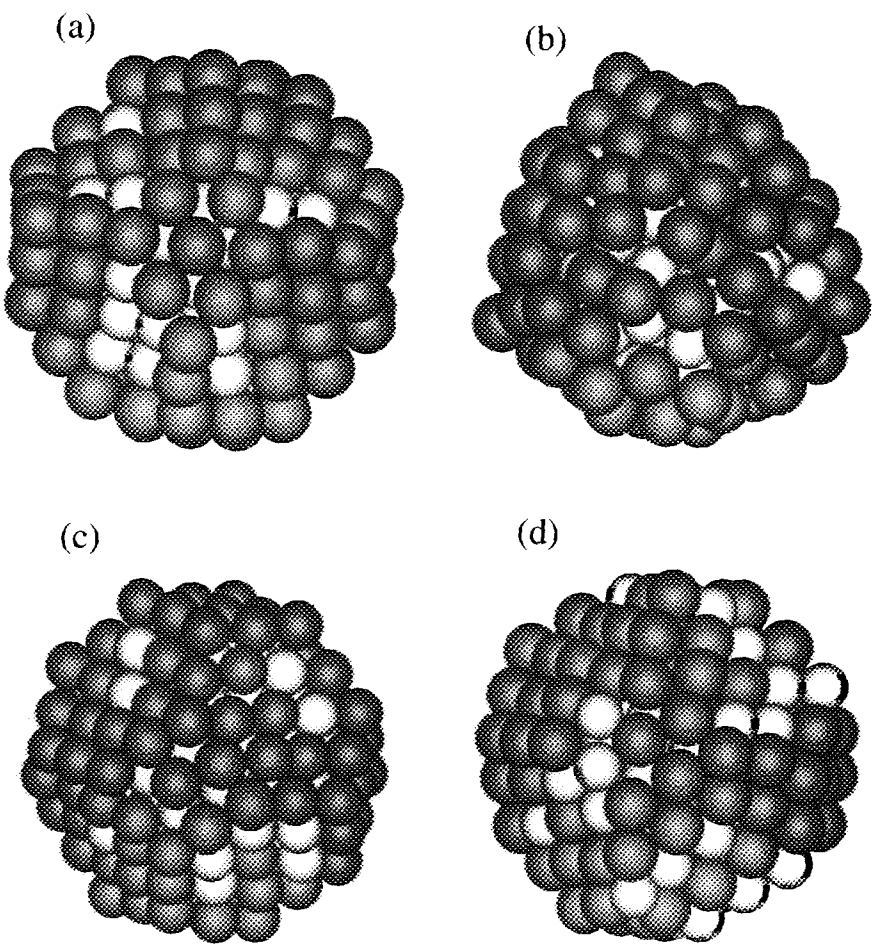

FIG. 2. Final configurations for 201-atom bimetallic clusters of (a) $Rh_{0.5}$–$Ag_{0.5}$, (b) $Ni_{0.5}$–$Ag_{0.5}$, (c) $Ni_{0.5}$–$Cu_{0.5}$, and (d) $Ni_{0.5}$–$Pd_{0.5}$, obtained from atomistic simulations at 600 K using the MD/MC-CEM potentials (14). The metal with higher surface energy is listed first, shown as brighter spheres, and depleted from the surface.

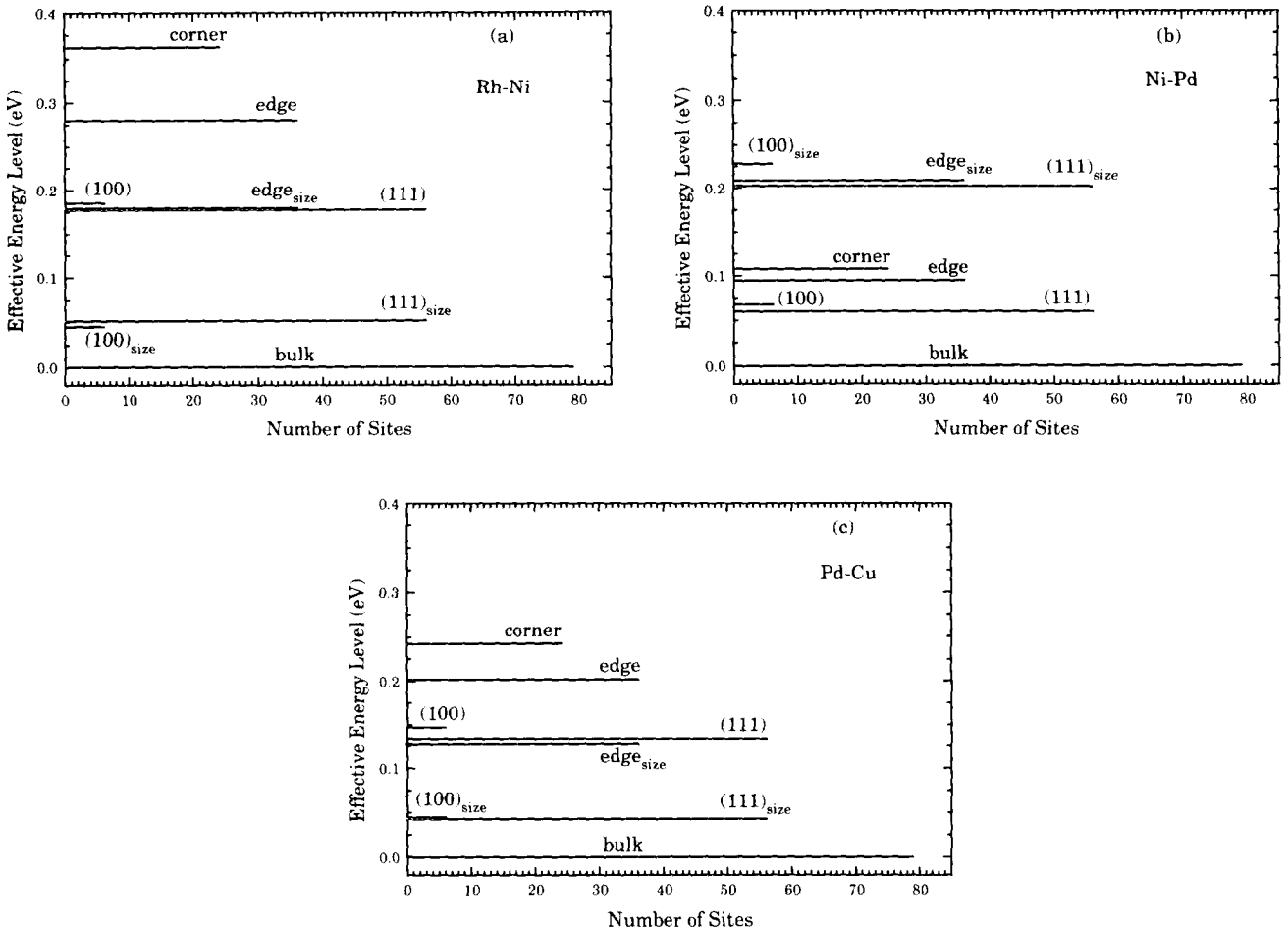

FIG. 3. MD/MC-CEM effective energy diagrams for 201-atom clusters of (a) Rh–Ni, (b) Ni–Pd, and (c) Pd–Cu, both without size effect and with size effect for a 50%–50% composition.

much *greater* than that in Rh–Ni (32%) and that in Pd–Cu (34%). This qualitative conclusion from the model with size effect is supported by the atomistic simulations. The simulations indicate that the surface segregation in Ni–Pd (31%) is indeed much *stronger* (not weaker) than that in Rh–Ni (40%) and that in Pd–Cu (39%).

With the above general trends in mind, we now proceed to the detailed comparison of the two models for the three more interesting systems in the fourth class. Presented in Fig. 3 are the effective energy levels for Rh–Ni (Fig. 3a), Ni–Pd (Fig. 3b), and Pd–Cu (Fig. 3c). Notice that Rh, Ni, and Pd will be depleted at the surface and edge–corner sites in the three systems, respectively. The (111), (100), and edge levels in Fig. 3b are lower than those in Figs. 3a and 3c without the size effect, but the opposite is true with the size effect. It can be seen from Fig. 3b that the size effect (i.e., Pd is *larger* than Ni) assists the energetic driving force for surface segregation in Ni–Pd (i.e., Pd also has a *lower* surface energy than Ni). In the Rh–Ni (Fig. 3a) and Pd–Cu (Fig. 3c) systems, the size effect opposes the energetic driving force since the larger atom has a *higher* surface energy.

Corresponding to Fig. 3, the surface segregation curves for 600 K obtained from the models are shown in Fig. 4, along with the results from atomistic simulations of 201-atom $Rh_{0.5}Ni_{0.5}$, $Ni_{0.5}Pd_{0.5}$, and $Pd_{0.5}Cu_{0.5}$ clusters using the MD/MC-CEM potential (14). Figures 4a (Rh–Ni) and 4c (Pd–Cu) suggest that the present empirical description underestimates the size effect, while Fig. 4b (Ni–Pd) suggests an overestimation. Two possible methods to improve the agreement between the model and the simulations are to vary the exponents, d_i's, in Eq. [10], and to try other forms for $\langle a_0 \rangle$ in Eq. [11]. Such changes will make the size effect either more pronounced or less pronounced in *all* bimetallic clusters thereby worsening the agreement in at least some systems. As such, it appears that the present choice for d_i's and $\langle a_0 \rangle$ may represent a very good compromise when all systems are considered.

Another point is that the simulated results are consistently closer to the nonsegregation line, the diagonal, than

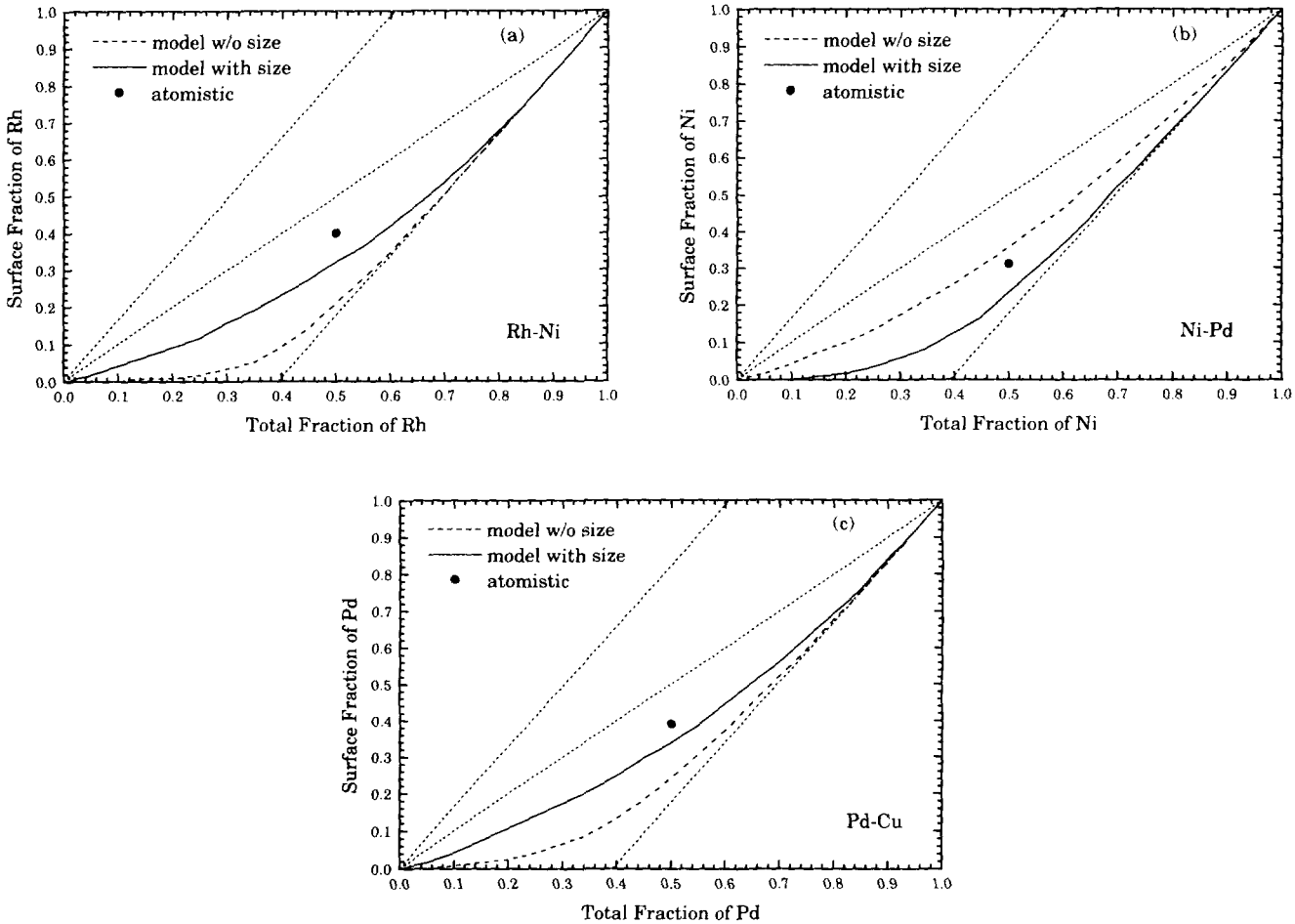

FIG. 4. Surface fractions in 201-atom clusters at 600 K for (a) Rh in Rh–Ni, (b) Ni in Ni–Pd, and (c) Pd in Pd–Cu. The curves are from the models while the solid circles are from atomistic simulations using the MD/MC-CEM potentials (14). The two parallel short-dashed lines encase the total allowable region of segregation, and the third short-dashed line (the diagonal) separates the enrichment (above) and depletion (below) regions.

the model with size effect. We believe that the major reason for this systematic difference is the neglect of the heat of mixing in the models. The MD/MC-CEM heats of mixing are -27, -12, and -18 meV/atom for bulk ordered 50%–50% alloys of Rh–Ni, Ni–Pd, and Pd–Cu, respectively (20). These values also change by 10–20 meV/atom for different compositions (20). Such energies are quite significant on the scale of Figs. 3a–3c; and attractions between different types of atoms will decrease segregation. A few other possible reasons for the systematic difference are the neglect of the vibrational and anharmonic contributions to the entropy and the fact that there are more than five energy levels in real systems.

In Table 4, the simulations also predict weaker edge–corner segregation than the models for Rh–Ni and Pd–Cu systems, as expected from the heat of mixing arguments. For Ni–Pd, however, the simulation predicts stronger edge–corner segreation (27%) than the model with size effect included (32%). This is due to the corner site energy level for Ni being lower than three other levels in the model with size effect (see Fig. 3b). Figure 3b suggests that the enrichment of Ni at the corners in Ni–Pd causes the decrease of the overall edge–corner segregation. Detailed results of the model with size effect show that the corner fraction of Ni in Ni–Pd is 58%, indeed larger than the total fraction of Ni which is 50%.

Now let us turn to the comparison of CEM (not MD/MC-CEM) results generated from the models and simulations. Shown in Fig. 5 are the effective energy levels for Rh–Pt generated using the CEM site energies in Table 3. Using both models, we obtained the surface fractions of Rh shown in Fig. 6. The model using Eq. [10], with size effect, produces edge–corner fractions for Rh as shown in Fig. 7. Since the lattice size mismatch is only 3% for Rh–Pt, the inclusion of size effect is not as important as in the previous focus examples, but is still noticeable in Fig. 6 due to the small spacing in effective energies in Fig. 5. Results of the atomistic simulation using the CEM

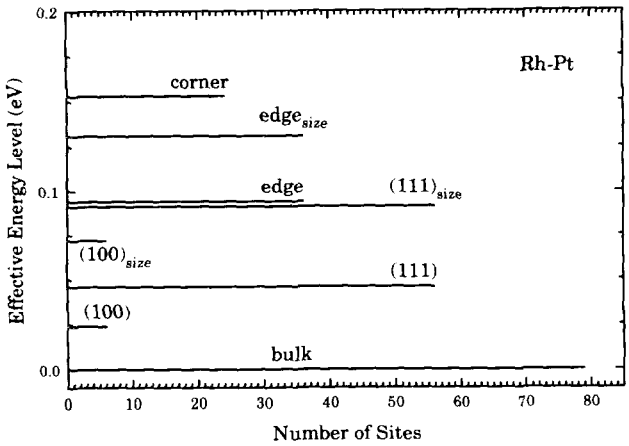

FIG. 5. CEM effective energy diagrams for 201-atom Rh–Pt clusters, both without size effect and with size effect for a 50%–50% composition.

potential (11, 13) are also shown in Figs. 6 and 7. The simulated result for surface segregation is again much closer to the nonsegregation line as compared to the model with size effect. The CEM heat of mixing for Rh–Pt is also slightly negative, −2.2 kJ/mol or −23 meV/atom for the bulk alloy (11, 13); thus, it is understandable that the simulated result shows less segregation.

We should point out that the CEM simulated results in Figs. 6 and 7 are much less reliable statistically, as compared to the MD/MC-CEM results in Fig. 4. Therefore, in the particular case of Fig. 6 only, another reason for the higher surface percentage for Rh in Rh–Pt could be a result of insufficient simulation time. As such, the quantitative agreement between the simulation and the model in Fig. 7 is likely fortuitous. Generally, the discrepancy between models and simulations is slightly larger for edge–corner segregation than for overall surface segregation, as shown in Table 4.

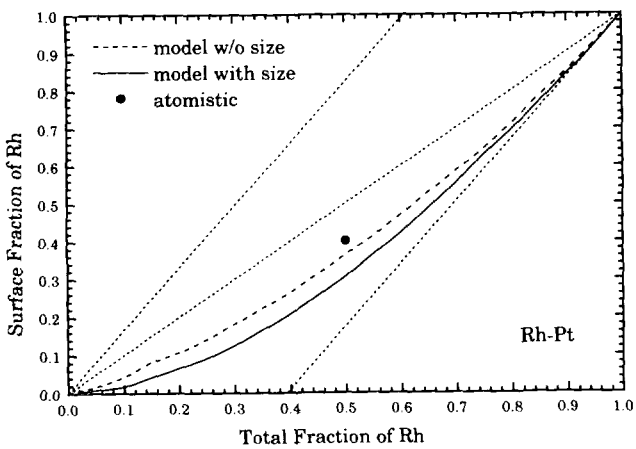

FIG. 6. Surface fractions of Rh in 201-atom Rh–Pt clusters at 600 K. The curves are from the models, while the solid circle is from atomistic simulations using the CEM potentials (11, 13).

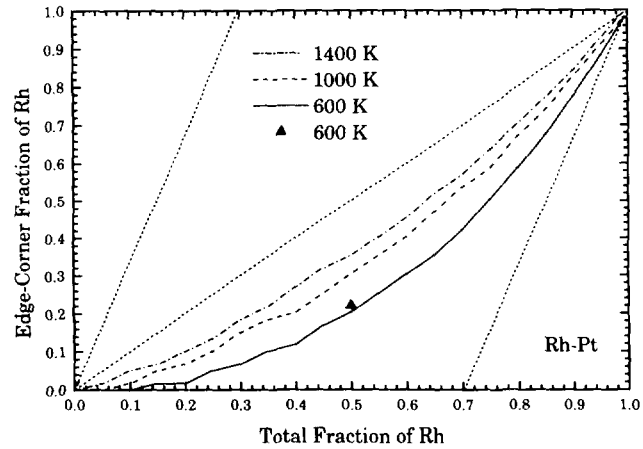

FIG. 7. Edge–corner fractions of Rh in 201-atom Rh–Pt clusters at 1400, 1000, and 600 K. The curves shown are from the model with size effect, while the solid triangle is from atomistic simulations using the CEM potentials (11, 13). The curves from the model without size effect (not shown) are nearly identical to the ones shown.

SUMMARY AND CONCLUSIONS

We applied a five-state statistical-mechanical model to study surface segregation in 201-atom bimetallic clusters of truncated cubo-octahedral shape. The effects of size mismatch between atoms of different type were included via a new empirical formula, based upon dimensional scaling arguments. Atoms of the same type and having the same number of nearest neighbors were assumed to have the same site energy, namely, the weighted average of the interaction energy per atom. Proper combination of these site energies then defined the "effective" energy levels of such a binary system. The site energies were extracted from the atomistic calculations of pure metal clusters of Al, Ni, Cu, Rh, Pd, Ag, Ir, Pt, and Au using the MD/MC-CEM theory and the CEM theory.

From the comparison of 201-, 586-, and 1289-atom clusters, we concluded that the lowest-coordination corner and edge site energies varied negligibly with cluster size. This implied that the statistical–mechanical model can be applied to clusters of any size using the site energies calculated from the small 201-atom clusters. Upon minimization of the free energy, the model reproduced qualitatively the surface segregation results generated by atomistic simulations at 600 K that we reported earlier, using both CEM and MD/MC-CEM theories. The inclusion of the size effect was shown to be important in a number of cases with the size corrected model providing better accuracy in 75% of the cases for surface segregation, but worse accuracy in 66% of the cases for edge–corner segregation, as compared to the model without size correction.

The model suffers from two main limitations. First, it does not incorporate a nonzero heat of mixing. Second,

it cannot treat systems with very large ($\geq$12.5%) lattice-size mismatch. Although the latter can be overcome only by performing atomistic simulations, the former may be overcome by improving the model in the future. Such an effort will allow more realistic treatment of many bi- and multimetallic clusters at negligible computational expense.

ACKNOWLEDGMENTS

The authors thank Professor T. S. King and Dr. T. J. Raeker for discussions. This work was supported by the Biological and Chemical Technologies Research Program (Advanced Industrial Concepts Division) of the U.S. Department of Energy through the Ames Laboratory, which is operated for the U.S. DOE by Iowa State University under Contract W-7405-Eng-82. The more extensive CEM calculations were performed on the nCUBE 2 hypercube at the Scalable Computing Laboratory of Iowa State University and the Ames Laboratory.

REFERENCES

1. Sinfelt, J. H., "Bimetallic Catalysts: Discoveries, Concepts and Applications." Wiley, New York, 1983.
2. Taylor, K. C., "Automobile Catalytic Converters." Springer, New York, 1984.
3. Dowben, P. A., and Miller, A. (Eds.), "Surface Segregation Phenomena." CRC Press, Boca Raton, FL, 1990.
4. Johnson, W. C., and Blakely, J. M. (Eds.), "Interfacial Segregation." American Society for Metals, Metals Park, OH, 1979.
5. Williams, F. L., and Nason, D., *Surf. Sci.* **45,** 377 (1974).
6. Burton, J. J., Hyman, E., and Fedak, D. G., *J. Catal.* **37,** 106 (1975).
7. Montejano-Carrizales, J. M., and Morán-López, J. L., *Surf. Sci.* **239,** 169 (1990); **239,** 178 (1990); **265,** 209 (1992).
8. Modak, S., and Khanra, B. C., *Solid State Commun.* **84,** 663 (1992).
9. Sundaram, V. S., and Wynblatt, P., *Surf. Sci.* **52,** 569 (1975).
10. Strohl, J. K., and King, T. S., *J. Catal.* **116,** 540 (1989).
11. Schoeb, A. M., Raeker, T. J., Yang, L., Wu, X., King, T. S., and DePristo, A. E., *Surf. Sci. Lett.* **278,** L125 (1992).
12. Tsai, N. H., Abraham, F. F., and Pound, G. M., *Surf. Sci.* **77,** 465 (1978).
13. Yang, L., Raeker, T. J., Schoeb, A. M., Wu, X., King, T. S., and DePristo, A. E., *Prepr. Am. Chem. Soc. Div. Fuel Chem.* **37,** 324 (1992).
14. Yang, L., Raeker, T. J., and DePristo, A. E., *Surf. Sci.* **290,** 195 (1993).
15. (a) Kress, J. D., and DePristo, A. E., *J. Chem. Phys.* **87,** 4700 (1987); (b) Kress, J. D., and DePristo, A. E., *J. Chem. Phys.* **88,** 2596 (1988); (c) Kress, J. D., Stave, M. S., and DePristo, A. E., *J. Phys. Chem.* **93,** 1556 (1989); (d) Stave, M. S., Sanders, D. E., Raeker, T. J., and DePristo, A. E., *J. Chem. Phys.* **93,** 4413 (1990); (e) Raeker, T. J., and DePristo, A. E., *Int. Rev. Phys. Chem.* **10,** 1 (1991); (f) Sinnott, S. B., Stave M. S., Raeker, T. J., and DePristo, A. E., *Phys. Rev. B* **44,** 8927 (1991); (g) Kelchner, C. L., Halstead, D. M., Perkins, L. S., and DePristo, A. E., *Surf. Sci.* **310,** 425 (1994).
16. Helms, C. R., *in* [4, Sect. II] (1979).
17. Strohl, J. K., and King, T. S., *J. Catal.* **118,** 53 (1989).
18. King, T. S., *in* [3, chap. 2] (1990).
19. Clementi, E., *IBM J. Res. Dev. Suppl.* **9** (1965); Bagus, P. S., Gilbert, T. L., and Roothan, C. J., *J. Chem. Phys.* **56,** 5195 (1972).
20. Raeker T. J., and DePristo, A. E., *Phys. Rev. B* **49,** 8663 (1994).